MULTIBODY DYNAMICS 2009, ECCOMAS Thematic Conference
K. Arczewski, J. Frączek, M. Wojtyra (eds.)
Warsaw, Poland, 29 June–2 July 2009

BEAM BENCHMARK PROBLEMS FOR VALIDATION OF FLEXIBLE MULTIBODY DYNAMICS CODES

A. L. Schwab[♮] and J. P. Meijaard[♯]

[♮]Laboratory for Engineering Mechanics
Delft University of Technology
Mekelweg 2, NL 2628 CD Delft, The Netherlands
e-mail: a.l.schwab@tudelft.nl

[♯]Faculty of Engineering Technology
University of Twente, Enschede, The Netherlands
e-mail: j.p.meijaard@utwente.nl

Keywords: Flexible Beams, Curved Beams, Buckling, Eigenfrequencies, Benchmark.

Abstract. *In this paper a set of benchmark problems involving flexible beams embedded in a multibody dynamics system are presented. The need for these benchmarks arises in the development of correct and accurate models of flexible bodies undergoing large displacements and large rotations. These can be used to test different formulations and implementations.*

A set of relatively simple problems are defined which comprise linear static, non-linear static, buckling and eigenfrequency analyses. The beams are either straight or initially curved. A complete specification of the problems is given. Solution sobtained by two versions of a spatial beam element and analytic solutions if available are presented as a reference.

1 INTRODUCTION

Since the introduction of computer codes for the analysis of flexible multibody dynamics systems, developers have been in need of testing the accuracy and restrictions of their codes by means of benchmark problems. One of the most challenging tasks within these codes is the correct and accurate modelling of spatial flexible bodies undergoing large displacements and large rotations. Although much is already known from the finite element method (FEM) world, these developments are often restricted to small displacement and small rotations, and were primarily developed for static analysis.

With the numerous codes available today, there are almost as many different benchmark problems as there are codes. One of the first flexible multibody dynamics benchmark problem was probably the analysis of a planar flexible four bar mechanism by Bahgat and Willmert (1976). Other well-known multibody dynamics problems are the dynamic analysis of a planar crank–slider mechanism with elastic connecting rod by Chu and Pan (1975) and Song and Haug (1980), the planar beam spin-up manoeuvre by Kane *et al.* (1987) which was part of a space based robot manipulator, the planar beam spin-up by Wu and Haug (1988), the spatial flying spaghetti by Simo and Vu-Quoc (1988), the spatial crank–slider mechanism with compliant connecting rod by Yoo and Haug (1986), the planar falling pendulum by Yakoub and Shabana (2001), and the spatial falling plate by Mikkola and Shabana (2003).

A first step in standardization of multibody dynamics benchmark problems was made by Gonzalez *et al.* (2006). Although in their guidelines they mention the need for extending the benchmark problems with good test cases, including flexible bodies, the paper only treats rigid multibody dynamics systems. This paper is a first step in extending the benchmark problems to flexible mutibody systems. Most of the existing benchmark problems in flexible multibody dynamics, although stylized, suffer from complexity. That is, if the results are not identical it is often hard to identify the underlying problem. Therefore we propose to introduce some basic benchmark problems for which analytic solutions are mostly known.

Flexible bodies can often by approximated by plate- or beam-like structures, meaning that one or two dimensions are small in comparison with the rest. Therefore, as a first start, we have developed a set of benchmark problems which validate the behaviour of spatial flexible beams within a multibody dynamics environment. Some earlier results are reported in Meijaard (1996) and Schwab and Meijaard (2005).

2 BEAM BENCHMARK PROBLEMS

The spatial beam benchmark problems focus on the correct formulation of slender beam elements undergoing large displacements and large rotations, but restricted to small deformations. Some attention is given to initially curved beams.

The benchmark problems start with simple static analyses in the small displacement regime to validate the correct formulation of the elastic forces. Next, a number of static large displacement and large rotation tests are performed on a straight and an initially curved beam. Then a number of buckling tests, normal, lateral, and torsional, are performed to check the way in which geometric stiffness due to pre-stress is taken into account. Then a number of eigenfrequency analyses are preformed to validate the combination of elastic forces and distributed inertia forces. These eigenfrequency tests are particularly useful because the results, eigenfrequencies and eigenmodes, are independent of the choice of coordinates. Finally, the effect of tensile pre-stress on the eigenfrequencies is investigated. In all tests the convergence of the results due to mesh refinement is investigated.

The benchmark problems described above are demonstrated on two variants of a classical Timoshenko beam with large displacement and large rotation formulation (Meijaard (1996)) as implemented in the multibody dynamics program SPACAR (Jonker and Meijaard (1990)). This finite beam element is a shear flexible beam based on the elastic line concept. This supposes that the beam is slender and the cross-section is doubly symmetric. Large displacements and rotations are allowed, but the deformations must remain small. The configuration of the element is determined by the positions and orientations of the two end nodes, by which it can be coupled to and interact with other elements. The positions of the end nodes p and q are given by their coordinates $\mathbf{x}^p$ and $\mathbf{x}^q$ in a global inertial system $Oxyz$. The change in orientation of a node with respect to the reference orientation is determined by an orthogonal rotation matrix $\mathbf{R}(\boldsymbol{\vartheta})$, which can be parametrized by a choice of parameters, denoted by $\boldsymbol{\vartheta}$, such as Euler angles, modified Euler angles, Rodrigues parameters and Euler parameters. We use Euler parameters with a constraint, but this choice is immaterial to the description of the properties of the element. For a beam element, orthogonal triads of unit vectors $(\mathbf{e}_x^p, \mathbf{e}_y^p, \mathbf{e}_z^p)$ and $(\mathbf{e}_x^q, \mathbf{e}_y^q, \mathbf{e}_z^q)$ rigidly attached to the nodes p and q respectively are defined. The unit vector $\mathbf{e}_x$ is perpendicular to the average warped cross-sectional plane of the beam in the sense of Cowper (1966), and $\mathbf{e}_y$ and $\mathbf{e}_z$ are in the principal directions of the cross-section. In the absence of shear deformations, $\mathbf{e}_x$ is tangent to the elastic line of the beam. The change in orientation of the triads is determined by the rotation matrix as $\mathbf{e} = \mathbf{R}(\boldsymbol{\vartheta})\bar{\mathbf{e}}$, where $\bar{\mathbf{e}}$ is a unit vector in the reference configuration.

The elastic forces are derived with the elastic line concept. The element has six degrees of freedom as a rigid body, while the nodes have twelve degrees of freedom. Hence the deformation that is determined by the end nodes of the element can be described by six independent generalized strains, which are functions of the positions and orientations of the nodes and the geometric parameters of the element. Two variants of the element are available. In the first, standard strain-displacement relations (continuity equations) are used, which is called BEAM. In he second variant, BEAMNL, additional quadratic terms in the strain-displacement relation are included to enhance the performance in the case of pre-stress. For the mass matrix a consistent mass formulation is used based on the elastic line concept (Meijaard (1996)), where rotary inertia of the cross-section can be lumped in the nodes.

The material used in the benchmark problems is isotropic and linearly elastic with modulus of elasticity $E = 210 \cdot 10^9$ N/m^2, Poisson ratio $\nu = 0.3$, shear modulus $G = E/(2(1+\nu))$, and density $\rho = 7850$ kg/m^3. The beam is initially aligned along the x-axis with the principal axes of the cross-section along the y- and z-axis. In the spirit of Euler, finite rotations are presented in the form of unit vector (e_x, e_y, e_z) and angle of rotation ϕ about the axis along this unit vector.

2.1 Small displacements and small rotations, cantilever beam

The first static benchmark is a small displacement and small rotation analysis of a cantilever beam loaded at the tip, see Figure 1. The beam has an undeformed length $l = 1$ m and the dimensions of the rectangular cross-section are $h = 0.02$ m and $w = 0.01$ m. The loads at the tip are a transverse force $F_z = 1 \cdot 10^{-4}$ N, a bending moment $M_y = 1 \cdot 10^{-4}$ Nm, and a torsional moment $M_x = 1 \cdot 10^{-4}$ Nm. The torsional stiffness of the rectangular cross-section is taken as $S_t = Ghw^3/3$. The theoretical results for the small displacements and small rotations at the tip are a tip displacement in the z-direction $u_z = F_z l^3/(3EI_y) - M_y l^2/(2EI_y)$, a rotation of the tip about the y-axis $\varphi_y = F_z l^2/(2EI_y) - M_y l/(EI_y)$, and a rotation of the tip about the x-axis $\varphi_x = M_x l/S_t$, where the remaining displacements and rotations are zero.

The numerical solution modelled by one BEAM element gives results with at least 6 significant digits compared to the theoretical solution.

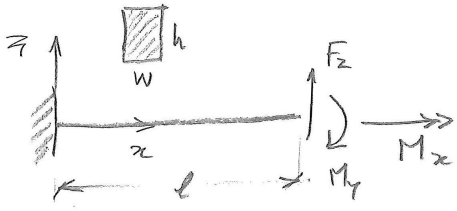

Figure 1: Cantilever beam.

2.2 Small displacements and small rotations, quarter circle beam

The second static benchmark is a small displacement and small rotation analysis of a cantilever quarter-circle beam loaded at the tip, see Figure 2. The undeformed radius of the quarter-circle is $R = 1$ m and the cross-section is circular with a diameter $d = 0.02$ m. The loads at the tip are a transverse force $F_z = 1 \cdot 10^{-4}$ N, and a moment $M_x = 1 \cdot 10^{-4}$ Nm. The torsional stiffness of the cross-section is taken as $S_t = (\pi/32)Gd^4$. The theoretical results for the small displacements and small rotations at the tip are

$$\begin{aligned} u_z &= \frac{F_z R^3}{4}\left(\frac{\pi}{EI_y} + \frac{3\pi - 8}{St}\right) + \frac{M_x R^2}{2}\left(\frac{1}{EI_y} + \frac{1}{S_t}\right), \\ \varphi_x &= \frac{F_z R^2}{2}\left(\frac{1}{EI_y} + \frac{1}{S_t}\right) + \frac{\pi M_x R}{4}\left(\frac{1}{EI_y} + \frac{1}{S_t}\right), \\ \varphi_y &= \frac{F_z R^2}{4}\left(\frac{4 - \pi}{S_t} - \frac{\pi}{EI_y}\right) + \frac{M_x R}{2}\left(\frac{1}{S_t} - \frac{1}{EI_y}\right). \end{aligned} \tag{1}$$

The initial curvature for the BEAM element is taken into account by adding an appropriate initial undeformed strain to the generalized bending strain expressions. Results for the BEAM element are shown in Table 1. The convergence rate is quadratic. Note that the circular arc approximation leads to an overestimation of the stiffness in the z-direction.

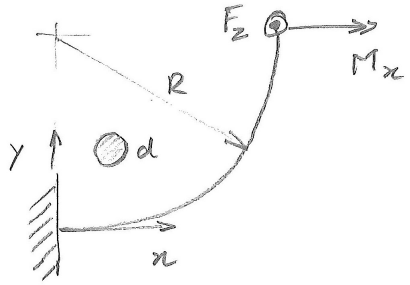

Figure 2: Quarter-circle beam.

2.3 Large displacements and large rotations, cantilever beam

The third static benchmark is a large displacement and large rotation analysis of a cantilever beam loaded at the tip, see Figure 1. The beam has an undeformed length $l = 1$ m and the dimensions of the rectangular cross-section are $h = 0.02$ m and $w = 0.005$ m. The loads at the tip are a bending moment $M_y = 100$ Nm, and a torsional moment $M_x = 25$ Nm. The

Table 1: Dimensionless tip displacement, $\bar{u}_z$, and dimensionless tip rotations, $\bar{\varphi}_x$ and $\bar{\varphi}_y$, for a cantilever quarter-circle beam loaded by a transverse force F_z and a moment M_x at the tip where the beam is divided into a number of BEAM elements of equal length. Displacements are non-dimensionalized by the theoretical values from (1).

number of	F_z			M_x		
elements	$\bar{u}_z$	$\bar{\varphi}_x$	$\bar{\varphi}_y$	$\bar{u}_z$	$\bar{\varphi}_x$	$\bar{\varphi}_y$
1	0.75518	0.61488	1.39630	0.61488	1.40919	7.54247
2	0.94638	0.97743	1.03461	0.97743	1.06900	1.88713
4	0.98744	0.99679	1.00609	0.99679	1.01581	1.19440
8	0.99692	0.99933	1.00138	0.99933	1.00387	1.04708
16	0.99923	0.99984	1.00034	0.99984	1.00096	1.01168
32	0.99981	0.99996	1.00008	0.99996	1.00024	1.00291

torsional stiffness of the rectangular cross-section is taken as $S_t = Ghw^3/3$. Results for the BEAM element are shown in Table 2. The convergence rate is quadratic.

Table 2: Tip displacements (u_x, u_y, u_z), and axis-angle tip rotation (e_x, e_y, e_z, φ) for a cantilever beam loaded by a a bending moment $M_y = 100$ Nm, and a torsional moment $M_x = 25$ Nm at the tip where the beam is divided into a number of BEAM elements of equal length.

number of							
elements	u_x [m]	u_y [m]	u_z [m]	e_x	e_y	e_z	φ [rad]
2	-0.26535	-0.58038	-0.10839	-0.09369	0.22896	-0.96892	1.29676
4	-0.22751	-0.52344	-0.11870	-0.05070	0.24360	-0.96855	1.19382
8	-0.22037	-0.51231	-0.11918	-0.04457	0.24617	-0.96820	1.17157
16	-0.21870	-0.50966	-0.11925	-0.04318	0.24679	-0.96811	1.16621
32	-0.21829	-0.50901	-0.11926	-0.04284	0.24695	-0.96808	1.16488

2.4 Large displacements and large rotations, quarter circle beam

The fourth static benchmark is a large displacement and large rotation analysis of a cantilever quarter-circle beam loaded at the tip, see Figure 2 . The undeformed radius of the quarter-circle is $R = 1$ m and the dimensions of the rectangular cross-section are $h = 0.02$ m and $w = 0.005$ m. The loads at the tip are a transverse force $F_z = 50$ N, and a moment $M_x = 50$ Nm. The torsional stiffness of the cross-section is taken as $S_t = Ghw^3/3$. Results for the BEAM element are shown in Table 3. The convergence rate is quadratic. Note that the displacements and rotations are overestimated.

Table 3: Tip displacements (u_x, u_y, u_z), and axis-angle tip rotation (e_x, e_y, e_z, φ) for a cantilever quarter-circle beam loaded at the tip by a transverse force $F_z = 50$ N, and a moment $M_x = 50$ Nm where the beam is divided into a number of BEAM elements of equal length.

number of							
elements	u_x [m]	u_y [m]	u_z [m]	e_x	e_y	e_z	φ [rad]
4	-0.40626	-0.24861	0.77679	-0.00165	-0.82599	0.56369	1.33316
8	-0.30544	-0.18640	0.68800	0.06638	-0.84045	0.53781	1.14212
16	-0.28894	-0.18083	0.67622	0.07743	-0.84454	0.52987	1.11342
32	-0.28508	-0.17966	0.67355	0.08002	-0.84555	0.52786	1.10678

2.5 Euler buckling, cantilever beam

In a linear buckling problem, the critical load mulipliers λ are determined by solving the generalized eigenvalue problem, $\det(\mathbf{K}_0 + \lambda \mathbf{K}_g) = 0$. Here, $\mathbf{K}_0$ is the linear stiffness matrix and $\mathbf{K}_g$ is the geometric stiffness matrix due to a reference load.

The first buckling benchmark is Euler or normal load buckling of a cantilever beam where the beam is loaded by a compressive normal force F_x at the tip, see Figure 3. The beam has an undeformed length $l = 1$ m and the dimensions of the rectangular cross-section are $h = 0.02$ m and $w = 0.01$ m. The theoretical Euler buckling load is $F_{th} = (\pi^2/4)(EI_{min}/l^2)$. Numerical

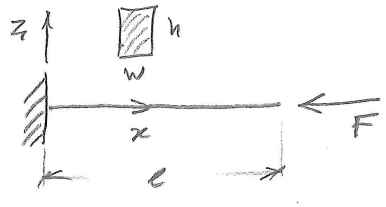

Figure 3: Euler buckling of a cantilever beam.

results for the buckling load F_{cr} are obtained for two types of elements, BEAM and BEAMNL, where the beam is divided in a number of elements of equal length, see Table 4. Note that the convergence rate is quadratic for BEAM elements and quartic for BEAMNL elements. Even if a single BEAMNL element is used a fairly accurate result is obtained.

Table 4: Critical Euler buckling load of a cantilever beam for two types of elements.

number of elements	BEAM F_{cr}/F_{th}	BEAMNL F_{cr}/F_{th}
1	1.215854	1.007522327
2	1.052387	1.000512141
4	1.012916	1.000032766
8	1.003217	1.000002060
16	1.000803	1.000000129
32	1.000201	1.000000008

2.6 Lateral buckling, cantilever beam

The second buckling benchmark is lateral buckling of a cantilever beam loaded by a lateral force F_z at the tip, see Figure 4. The beam has an undeformed length $l = 1$ m and the dimensions of the rectangular cross-section are $h = 0.02$ m and $w = 0.002$ m. The theoretical lateral buckling load is $F_{th} = 4.012\ 599\ 344\ (EI_{min}S_t)^{1/2}/l^2$, where EI_{min} is the smaller flexural rigidity and $S_t = Ghw^3/3$ the torsional stiffness. Numerical results for the critical lateral buckling load F_{cr} are obtained for two types of elements, BEAM and BEAMNL, where the beam is divided into a number of elements of equal length, see Table 5. Note that the convergence rate is quadratic for both BEAM and BEAMNL elements, although the results for the BEAMNL elements are more accurate. The convergence rate for the BEAMNL element is only quadratic because the buckling mode involves torsion which is approximated by a linear rotation field.

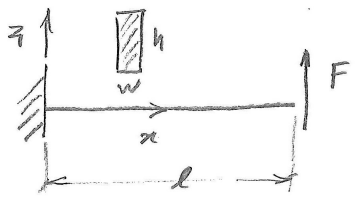

Figure 4: Lateral buckling of a cantilever beam.

Table 5: Critical lateral buckling load of a cantilever beam for two types of elements.

number of elements	BEAM F_{cr}/F_{th}	BEAMNL F_{cr}/F_{th}
1	Inf	1.495290
2	1.220899	1.069138
4	1.046009	1.015367
8	1.011215	1.003862
16	1.002788	1.000969
32	1.000696	1.000243

2.7 Torque buckling, cantilever beam

The third buckling benchmark is torque buckling of a cantilever beam by a torsion moment M_x at the tip, see Figure 5. The beam has an undeformed length $l = 1$ m and the dimension of the circular cross-section is $d = 0.02$ m. If the torsion moment is semitangential, the theoretical torque buckling load is $M_{th} = \pi EI/l$ (Ziegler (1968)), where EI is the flexural rigidity. Numerical results for the critical torque buckling load M_{cr} are obtained for two types of ele-

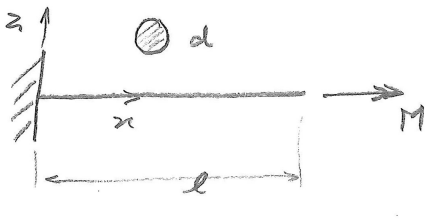

Figure 5: Torque buckling of a cantilever beam.

ments, BEAM and BEAMNL, where the beam is divided into a number of elements of equal length, see Table 6. Note that the convergence rate is quadratic for BEAM elements and quartic for BEAMNL elements, since the buckling mode only involves bending.

2.8 Eigenfrequencies of a free beam

In an eigenfrequency analysis, the eigenfrequencies ω are determined by solving the generalized eigenvalue problem $\det(\mathbf{K} - \omega^2\mathbf{M}) = 0$. Here, $\mathbf{K}$ is the tangent stiffness matrix and $\mathbf{M}$ is the mass matrix.

The first dynamic benchmark is the eigenfrequency analysis for a free vibrating beam. The beam has an undeformed length $l = 1$ m and the dimensions of the square cross-section are $w = h = 0.02$ m. For the torsional stiffness we use $S_t = Gk_xI_p$, with the shear distribution

Table 6: Critical torque buckling load of a cantilever beam for two types of elements.

number of elements	BEAM M_{cr}/M_{th}	BEAMNL M_{cr}/M_{th}
1	Inf	1.102657791
2	1.273240	1.007498979
4	1.054786	1.000510386
8	1.013052	1.000032732
16	1.003225	1.000002060
32	1.000804	1.000000129

factor $k_x = 0.8436$ from Timoshenko and Goodier (1987), and the polar area moment of inertia is $I_p = I_y + I_z$. For the mass distribution the consistent mass matrix is used, where the rotary inertia about the longitudinal axis is lumped in the nodes.

The theoretical eigenfrequencies are for the first longitudinal mode $\omega_L = \pi\sqrt{E/(\rho l^2)}$, the first torsional mode $\omega_T = \pi\sqrt{k_x G/(\rho l^2)}$, and the first and second bending mode $\omega_{B1} = 22.373\,285\,448\,\sqrt{EI_y/(\rho A l^4)}$ and $\omega_{B2} = 61.672\,822\,873\,\sqrt{EI_y/(\rho A l^4)}$.

The non-zero dimensionless eigenfrequencies are presented in Table 7. The zero eigenvalues are not reported since both types of beam elements describes the rigid body modes exactly. The eigenfrequencies are non-dimensionalized by the theoretic values. Note that the convergence rate is quadratic for the longitudinal and the torsional modes and quartic for the bending modes.

Table 7: Dimensionless eigenfrequencies for a free vibrating beam modelled by a number of equal-length BEAM elements. The eigenfrequencies are non-dimensionalized by the theoretic values.

number of elements	Longitudinal $\bar{\omega}_L$	Torsional $\bar{\omega}_T$	First Bending $\bar{\omega}_{B1}$	Second Bending $\bar{\omega}_{B2}$
1	0.913460	0.636618	1.199323890	1.486092409
2	1.044582	0.900315	1.002233033	1.137900472
4	1.013405	0.974494	1.001087275	1.006226715
8	1.003456	0.993585	1.000080650	1.000583565
16	1.000870	0.998394	1.000005238	1.000039344
32	1.000218	0.999597	1.000000330	1.000002504

2.9 Eigenfrequencies of a simply supported beam with pre-stress

The second dynamic benchmark is the eigenfrequency analysis for the vibration of a simply supported beam with tensile pre-stress. The beam has an undeformed length $l = 1$ m and the dimensions of the square cross-section are $w = h = 0.02$ m. For the mass distribution the consistent mass matrix is used.

The theoretical value for the first bending eigenfrequency is $\omega_{Bth} = \omega_0\sqrt{1+\alpha}$, with the zero-load eigenfrequency $\omega_0 = \pi^2\sqrt{EI_y/(\rho A l^4)}$ and the non-dimensional pre-stress $\alpha = Fl^2/(\pi^2 EI_y)$.

The dimensionless eigenfrequencies for the BEAM element model are presented in Table 8 for a number of increasing levels of pre-stress. The eigenfrequencies are non-dimensionalized by the theoretic values. Note the quartic convergence rate at zero pre-stress and the nearly quadratic convergence rate at high pre-stress. Results for the same problem but now modelled

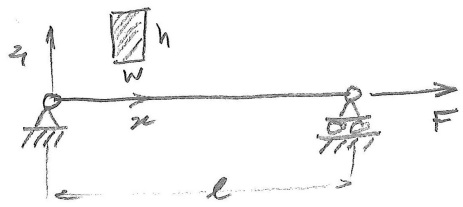

Figure 6: Simply supported beam with tensile pre-stress for eigenfrequency analysis.

Table 8: Dimensionless first bending eigenfrequency ω_B/ω_{Bth} for a simply supported beam with pre-stress F, modelled by a number of equal-length BEAM elements for a number of pre-stress levels $\alpha = Fl^2/(\pi^2 EI_y)$. The eigenfrequencies are non-dimensionalized by the theoretic values ω_{Bth}.

number of	α					
elements	0	0.01	0.1	1	10	100
1	1.109917957	1.104409645	1.058265	0.784831	0.334653	0.110441
2	1.003946897	1.003037064	0.995543	0.955757	0.893954	0.441764
4	1.000259662	1.000012707	0.997990	0.987691	0.976943	0.971028
8	1.000016443	0.999953309	0.999437	0.996823	0.994197	0.993616
16	1.000001031	0.999985158	0.999855	0.999199	0.998542	0.998411
32	1.000000064	0.999996092	0.999964	0.999799	0.999635	0.999603

with BEAMNL elements are shown in Table 9. The convergence rate is quartic irrespective of the level of pre-stress.

Table 9: Dimensionless first bending eigenfrequency ω_B/ω_{Bth} for a simply supported beam with pre-stress F, modelled by a number of equal-length BEAMNL elements for a number of pre-stress levels $\alpha = Fl^2/(\pi^2 EI_y)$. The eigenfrequencies are non-dimensionalized by the theoretic values ω_{Bth}.

number of	α					
elements	0	0.01	0.1	1	10	100
1	1.109917957	1.109818228	1.108929277	1.100816510	1.059172893	1.016296332
2	1.003946897	1.003943099	1.003909260	1.003601608	1.002054862	1.000504469
4	1.000259662	1.000259403	1.000257094	1.000236109	1.000130806	1.000026577
8	1.000016443	1.000016426	1.000016278	1.000014935	1.000008197	1.000001531
16	1.000001031	1.000001030	1.000001021	1.000000936	1.000000513	1.000000093
32	1.000000064	1.000000064	1.000000064	1.000000059	1.000000032	1.000000006

2.10 Eigenfrequencies of a rotating beam

The third and last dynamic benchmark is the eigenfrequency analysis of a beam rotating at a constant angular speed Ω, see Figure 7. The beam has an undeformed length $l = 1$ m and the dimensions of the rectangular cross-section are $h = 0.02$ m and $w = 0.2$ m. For the mass distribution the consistent mass matrix is used.

For a rotating beam there are two distinct bending vibrations. The bending vibration where the vibrating motion is perpendicular to the plane of rotation, here the xy-plane, is called the the flap mode, whereas the bending vibration in the plane of rotation is called the lead-lag mode. For the numerical model we calculate the first flap eigenfrequency and the first lead-lag eigenfrequency for a range of rotational speeds Ω. The eigenfrequency of the first flap

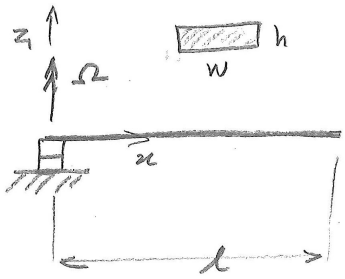

Figure 7: Rotating beam for eigenfrequency analysis.

mode ω_{FL} is non-dimensionalized by the theoretical first flap eigenfrequency at zero speed $\omega_{Byth} = 22.373\,285\,448\,\sqrt{EI_y/(\rho Al^4)}$ and likewise the first lead-lag frequency ω_{LL} is non-dimensionalized by $\omega_{Bzth} = 22.373\,285\,448\,\sqrt{EI_z/(\rho Al^4)}$. The rotational speed is chosen as $\Omega = \alpha\omega_{Byth}$, where α ranges from 0 to 100.

Table 10: Dimensionless first flap eigenfrequency $\omega_{FL}/\omega_{Byth}$ for a rotating beam modelled by a number of equal-length BEAM elements for a number rotational speed levels $\alpha = \Omega/\omega_{Byth}$. The eigenfrequencies are non-dimensionalized by the theoretic values ω_{Byth}.

number of	α					
elements	0	0.01	0.1	1	10	100
1	1.004754324	1.004806102	1.009918	1.427228	10.484302	104.260615
2	1.000483438	1.000537859	1.005911	1.442678	10.123374	100.434722
4	1.000032708	1.000090911	1.005836	1.466565	10.152925	100.070073
8	1.000002083	1.000061373	1.005913	1.473959	10.229131	100.040063
16	1.000000131	1.000059702	1.005939	1.475900	10.281906	100.066386
32	1.000000008	1.000059650	1.005946	1.476391	10.302030	100.122944

The dimensionless first flap eigenfrequency for the BEAM element model is presented in Table 10 for a number of increasing levels of rotational speed. The eigenfrequencies are non-dimensionalized by the theoretic value at zero speed. The convergence rate is quartic at zero speed and the nearly quadratic at high speed. For high rotation speeds the first flap eigenfrequency approaches the rotational speed. The first vibration mode has concentrated bending near the hub, whereas the rest of the beam nearly moves as a rigid body. However, at these high rotation speeds the model can be become unstable. This is due to the element near the tip for which the normal force vanishes at the tip. The unstable mode is therefore localized near the tip. This instability is only caused by the way the system is modelled and does not correspond to a real system instability. One way to avoid this problem would be to make the last element rigid.

Results for the same problem but now modelled with BEAMNL elements are shown in Table 11. Again the convergence rate is quartic at zero speed and nearly quadratic at high speed. However, the accuracy is much higher than for the BEAM element.

The dimensionless first lead-lag eigenfrequency for the BEAM element model are presented in Table 12 for a number of increasing levels of rotational speed. The eigenfrequencies are non-dimensionalized by the theoretic value at zero speed. Note the quartic convergence rate at zero speed and the nearly quadratic convergence rate at high speed. The first lead-lag eigenfrequency increases more slowly with increasing rotational speed than for the first flap eigenfrequency.

Results for the same problem but now modelled with BEAMNL elements are shown in Ta-

Table 11: Dimensionless first flap eigenfrequency as in Table 10 but now modelled by a number of BEAMNL elements.

number of	α					
elements	0	0.01	0.1	1	10	100
1	1.004754324	1.004818710	1.011172576	1.517142979	11.662928	115.589396
2	1.000483438	1.000543260	1.006447510	1.479078935	10.574380	104.878129
4	1.000032708	1.000092382	1.005981809	1.476709951	10.374878	102.296082
8	1.000002083	1.000061749	1.005950380	1.476564560	10.320334	101.153429
16	1.000000131	1.000059796	1.005948379	1.476555572	10.310803	100.623037
32	1.000000008	1.000059673	1.005948254	1.476555012	10.309830	100.396704

ble 13. Again, a quartic convergence rate at zero speed and a nearly quadratic convergence rate at high speed is observed.

Table 12: Dimensionless first lead-lag eigenfrequency $\omega_{LL}/\omega_{Bzth}$ for a rotating beam modelled by a number of equal-length BEAM elements for a number rotational speed levels $\alpha = \Omega/\omega_{Byth}$. The eigenfrequencies are non-dimensionalized by the theoretic values ω_{Bzth}.

number of	α					
elements	0	0.01	0.1	1	10	100
1	1.004754324	1.004754344	1.004756340	1.004955	1.018323	3.149731
2	1.000483438	1.000483482	1.000487885	1.000928	1.039866	1.575727
4	1.000032708	1.000032790	1.000040914	1.000852	1.072761	1.755588
8	1.000002083	1.000002176	1.000011375	1.000930	1.082847	2.152984
16	1.000000131	1.000000227	1.000009704	1.000956	1.085487	2.391194
32	1.000000008	1.000000105	1.000009652	1.000963	1.086155	2.476297

Table 13: Dimensionless first lead-lag eigenfrequency as in Table 12 but now modelled by a number of BEAMNL elements.

number of	α					
elements	0	0.01	0.1	1	10	100
1	1.004754324	1.004754470	1.004768949	1.006215682	1.140932	6.002008
2	1.000483438	1.000483536	1.000493286	1.001467229	1.089806	3.437691
4	1.000032708	1.000032805	1.000042385	1.000999212	1.086588	2.763748
8	1.000002083	1.000002180	1.000011751	1.000967626	1.086391	2.551374
16	1.000000131	1.000000228	1.000009798	1.000965615	1.086379	2.512544
32	1.000000008	1.000000105	1.000009675	1.000965489	1.086378	2.508545

3 CONCLUSIONS

In this paper some basic flexible beam benchmark problems have been presented. The set of problem comprises linear static, non-linear static, buckling and eigenfrequency problems. The set of problems is kept simple so a complete specification of the problems can be given. Numerical results, with two versions of a beam element, have been given with a sufficient number of significant digits so this can be used to compare results obtained by other methods.

References

Bahgat, B. M. and Willmert, K. D. (1976). Finite element vibrational analysis of planar mechanisms. *Mechanism and Machine Theory*, **11**, 47–71.

Chu, S. C. and Pan, K. C. (1975). Dynamic response of a high-speed slider-crank mechanism with an elastic connecting rod. *ASME Journal of Engineering for Industry*, **B97**, 542–550.

Cowper, G. R. (1966). The shear coefficient in Timoshenko's beam theory. *Journal of Applied Mechanics*, **33**, 335–340.

Gonzalez, M., Dopico, D., Lugris, U., and Cuadrado, J. (2006). A benchmarking system for MBS simulation software: Problem standardization and performance measurement. *Multibody System Dynamics*, **16**(2), 179–190.

Jonker, J. B. and Meijaard, J. P. (1990). SPACAR - Computer program for dynamic analysis of flexible spatial mechanisms and manipulators. In W. Schiehlen, editor, *Multibody systems handbook*, pages 123–143. Berlin, Germany: Springer.

Kane, T. R., Ryan, R. R., and Banerjee, A. K. (1987). Dynamics of a cantilever beam attached to a moving base. *AIAA Journal of Guidance, Control, and Dynamics*, **10**(2), 139–151.

Meijaard, J. P. (1996). Validation of flexible beam elements in dynamics programs. *Nonlinear Dynamics*, **9**, 21–36.

Mikkola, A. M. and Shabana, A. A. (2003). A non-incremental finite element procedure for the analysis of large deformation of plates and shells in mechanical system applications. *Multibody System Dynamics*, **9**, 283–309.

Schwab, A. L. and Meijaard, J. P. (2005). Comparison of three-dimensional flexible beam elements for dynamic analysis: finite element method and absolute nodal coordinate formulation. In *Proceedings of IDETC/CIE 2005, ASME 2005 International Design Engineering Technical Conferences & Computers and Information in Engineering Conference*, September 24-28, 2005, Long Beach, CA. ASME, New York. DETC2005-85104, 9p.

Simo, J. C. and Vu-Quoc, L. (1988). On the dynamics in space of rods undergoing large motions - a geometrically exact approach. *Computer Methods in Applied Mechanics and Engineering*, **66**(2), 125–161.

Song, J. O. and Haug, E. J. (1980). Dynamic analysis of planar flexible mechanisms. *Computer Methods in Applied Mechanics and Engineering*, **24**, 359–381.

Timoshenko, S. P. and Goodier, J. N. (1987). *Theory of Elasticity*. McGraw-Hill, New York.

Wu, S. C. and Haug, E. J. (1988). Geometric non-linear substructuring for dynamics of flexible mechanical systems. *International Journal for Numerical Methods in Engineering*, **26**(10), 2211–2226.

Yakoub, R. Y. and Shabana, A. A. (2001). Three dimensional absolute nodal coordinate formulation for beam elements: Implementation and applications. *Journal of Mechanical Design*, **123**(4), 614–621.

Yoo, W. S. and Haug, E. J. (1986). Dynamics of flexible mechanical systems using vibration and static correction modes. *Journal of Mechanisms, Transmissions and Automation in Design*, **108**, 315–322.

Ziegler, H. (1968). *Principles of Structural Stability*. Blaisdell,Waltham, Massachusettes.